DUMAND Cruise Report: Mechanical and Acoustic Studies of Deep Ocean Glass Sphere Implosions

Peter Gorham, Marc Rosen, Jeffrey Bolesta, and Joern Reise

August 19, 1992

Dept. of Physics and Astronomy, University of Hawaii
2505 Correa Rd., Honolulu, HI, 96822
(for the DUMAND Collaboration)

Abstract

Three deep-ocean implosions of 43 cm diameter glass instrument housings, made by Benthos Inc., were studied to determine the effect on their associated cabling and moorings. High resolution acoustic profiles were also measured for two of the three implosions, allowing us to infer some of the dynamics and kinematics of the events. The mechanical forces on the ancillary mooring hardware during the entire implosive/explosive event were found to be most probably dominated by the explosive shock wave following the initial infall. A syntactic float at a distance of 16 m from the implosion center was probably shattered by such a shock wave, but 3 glass instrument housings apparently survived within a distance of 6 m from the same implosion.

1 Introduction

Although many thousands of large spherical glass instrument housings have been deployed in the ocean, up to depths of 6 km or more, the statistics on failure of these housings under pressure are very poorly known. Sphere failures during test cycles after manufacture are very rare, and are most often traceable to flawed handling rather than inherent flaws in the glass itself. Records of sphere failure *in situ* are necessarily very incomplete; such failure can lead to loss of the instrument package and therefore no knowledge of the cause of the loss.

Because the failure rate in documented cases has been known to be primarily due to handling problems, it is virtually impossible to accurately estimate the likelihood of sphere failure in a large

array of many hundreds of instrument spheres deployed in the deep ocean over many years' time. Thus knowledge of the effects of such an implosion is useful in determining what measures must be taken to ensure survival of other instruments in the vicinity. (A review of the use of spherical glass housings in the deep ocean may be found in Raymond (1975)).

The Deep Underwater Muon and Neutrino Detector (DUMAND) will consist in its initial stage as an array of some 200 photomultipliers housed in 43 cm diameter glass spheres, and an additional $\sim$ 30 calibration spheres, bringing the total to $\sim$ 230. These instrument spheres are arrayed at 10 m intervals along 9 individual moorings, with total heights of 350 m, beginning at 100 m above the sea floor, and spaced at the center and vertices of an octagon with 40 m sides. The planned site is $\sim$ 20 km west of Keahole Point, Hawaii Island, at a depth of 4700 m. Because of the difficulty in assessing the likelihood of sphere failure, and the knowledge that at the working array depths each sphere has a potential energy of $\sim 1.5 \times 10^6$ Joule, we devised an experiment which could test the viability of the tensile mooring and the electro-optical power and telemetry riser cables for survival in the event of implosion. Since destruction of any of these three components could lead to failure of an entire instrument string, the experiment was designed to test a number of possible configurations which might mitigate such damage.

In addition to the photo-optical sensors in the array which are designed to detect Cherenkov emission from energetic charged particles which may be the interaction products of a primary neutrino, the DUMAND array will also contain an acoustic sub-array which is designed to track the positions of all of the sensors to $\sim$ 1 cm precision in real time. This acoustic sub-array will consist of $\sim$ 40 hydrophones, and a smaller subset of acoustic responder/transponders which use chirp techniques to range the hydrophones. Because of the potentially damaging strength that an acoustic pulse from an implosion might have for the hydrophone array, we also made surface recordings of the sound intensity. Although such measurements have been made in the past for deep-ocean implosions of similar housings (Orr and Schoenberg 1976), we have improved on the sampling interval by more than a factor of four; thus such measurements are of interest to those studying ocean acoustics, as well as the dynamics of implosive events.

2 Experimental Setup

As was shown in Orr and Schoenberg (1976), based on work done with the Benthos Corporation, glass instrument housings may be prepared in such a way that they will implode at a predetermined depth, by grinding a flat on a section of the sphere exterior. Three such spheres were used for this experiment, with the flat sizes chosen to implode at a depth of $\sim$ 4000 m. A cross-section of such a sphere is shown in Figure 1, with the wall thickness at the flat center as the indicated dimension. The ratio of this to the sphere radius is denoted the flat-thickness ratio (FTR).

It is standard practice in installation of oceanographic moorings to encase the instrument spheres within plastic hardhats. These are usually made of polyethylene or ABS plastic. The requirement for transparency in DUMAND has led us to the use of acrylic hardhats, primarily

because of the superior ultraviolet transmissivity of pure acrylic compared to most other clear plastics. However, acrylic hardhats are somewhat less mechanically robust than some other choices. For this experiment, a set of acrylic hardhats used in a previous ship-tethered DUMAND experiment were used (O'Connor 1990).

The initial experimental setup is shown in Fig. 2 (a). An aluminum frame made of T-bar stock was used to provide a tensioning jig so that the module vehicle could simulate the expected tension in the actual array ($\sim$ 5 KN per side). The side view of the implosion module does not show the mooring geometry, but this consists of a pair of kevlar risers, $\sim$ 12 mm diameter, with fiber optic and electrical cable bundles on both sides of this dual riser, each with diameters of order 2-3 cm. For the initial experiment, the kevlar risers and electro-optical cable bundle were encapsulated within a channel in the acrylic hardhat with some clamping pressure applied by the acrylic. Cross members in the tensioning frame were used to rotate the module 90° relative to the plane of the tensioning frame. This was done to minimize the effects of the T-bar frame on the implosion dynamics near the dual risers.

The experiment was designed as a free-fall vehicle, with two parallel mechanical anchor releases that could be activated either by loss of a small tether attached to the acrylic hardhat, or by a corrodible link. A concrete ballast with 400 lb wet weight was used to overcome the dual bouyancy packages: one using a pair of 43 cm glass floats (with a smaller transponder sphere mounted above them), the second a large syntactic foam float with approximately 20 lb lead counterballast to provide a righting moment.

As we will discuss in the following section, this initial package was lost in spite of the redundancy of releases and buoyancy in its design. A second package was assembled from the spares of the first package, as shown in Fig. 2 (b). This package did not include a tensioning frame, but did employ a protective titanium "picture frame" around the acrylic hardhat. This frame was a design chosen to provide as much protection as possible for the electro-optical riser cables. This was accomplished by terminating the kevlar tensile members at the corners of the Ti frame, while leading the electro-optical cables past the module on the outside face of a T-section of 1/8" titanium with the stem of the T facing the module. The twin halves of the acrylic hardhat then sandwiched the T-stock at this stem section, and were through-bolted to it with 1/4" bolts. Some of the bolts used for this were grade-8 high-tensile strength steel; others were mild steel. The titanium T-sections were stitch-welded 6Al4V alloy, with a tensile strength of order 120-130 KPSI.

The acoustic recording system consisted of a Marantz professional Digital Audio Tape (DAT) recorder, sampling at 48 KHz on dual channels with individually settable gains. The channels were set to attenuations of -20 dB and -60 dB relative to the nominal hydrophone gain. The hydrophone used was an Ocean and Atmospheric Science E-series model, with a sensitivity of -87 dB re 1 V per μPa. The variation of this sensitivity with frequency will be discussed below. The hydrophone was deployed on a weighted line with approximately 20 m of cable, at a depth of $\sim$ 5 m below the surface. Because of the sea state (Beaufort II-III) during most of the operations, the measurements were made with a slight way on to keep the vessel (a 43 foot fishing boat) head to the seas.

3 Observations

The tests were conducted approximately 6 miles SSW of the nominal DUMAND site, within a radius of 1.5 miles of 19° 39′ N 156° 20′ W, during the period 26-28 June 1992, in water depths ranging from 4.5-4.7 km. Three different implosions were successfully achieved at depth: the first with the package shown in Fig. 1(A), the second with that shown in Fig. 1(B), and the third an expendable package consisting only of a glass ball within a thin rubberized cloth bag tethered to a 400 lb wet-weight ballast.

3.1 First test

The initial package carried a Benthos XT-6000 transponder by which slant ranges to the descending instrument could be determined. After the package was released, the descent rate was determined to be ~ 1.4 m s^{-1}, and this rate continued until the implosion occured after a span of ~ 52 min. Shortly prior to the implosion, the hydrophone cable became entangled in the vessel's propellor, and it was not recovered and redeployed in time to record the first acoustic profile. However, divers present in the water at the time clearly heard the signal, and a transponder range was obtained immediately. This, combined with satellite navigation (GPS) positions obtained at the time, gave an implosion depth of 4140 ± 70 m, using a standard curve for the velocity of sound obtained in the same area (O'Connor 1990).

After the implosion occurred, transponder ranges were taken to determine whether the ballast releases had functioned successfully, and it was found that the package continued its descent. The descent rate had, however, slowed to ~ 0.5 m s^{-1}. This indicated that some significant change in net buoyancy had occurred, not due to the loss of buoyancy of the implosion sphere, since this would only increase the descent rate if the main ballast remained present. The package continued its descent until it rested on the bottom at a depth of approximately 4640 m. The survival of the transponder, contained within a smaller glass sphere directly adjacent to the 43 cm glass floats, strongly indicates that no sympathetic implosion took place among these floats, at a distance of ~ 6 m from the center of the imploding sphere.

During a return to station to compensate for drift approximately 5 hours following the implosion, one half of the top syntactic float was encountered on the surface. This was recovered, and examination of it indicated that it had been shattered, and the recovered section did not carry the righting ballast or the stainless steel attachment shaft. Two other smaller pieces of the float were also seen and recovered, both with similar shattered appearance. We surmise that the shatter of the float occurred as a result of the implosion-induced shock wave impact on the float, which had a flat surface area of order 1/3 m^2 facing directly at the imploding sphere, although it was ~ 16 m distant from it.

Although the remaining buoyancy of the two glass floats was estimated to be just sufficient to return the package to the surface, the fact that the syntactic float's righting ballast and associated

hardware remained attached to these spheres, while the syntactic float was entirely lost, probably accounts for the failure of this package to return. The change in fall rate mentioned previously suggests strongly that the anchor did release. Given the results of the following test it is difficult to imagine how the triggering scheme, which was based on fracture of the acrylic hardhat, could have failed to operate successfully.

3.2 Second Test

Once it became apparent that the secondary corrosion releases of the system were also unlikely to aid in returning the first package, we assembled a second free-fall package from the remaining spares, intending to still gather information on the implosion damage if possible. This package could not simulate the tensile riser tension, but did provide a reasonable simulation of the electro-optical riser configuration, since this is not under tension in the array design. As mentioned above, the acrylic hardhat in this case was captured within a rigid "picture frame" of titanium which was designed to survive even if the hardhat were destroyed. The release consisted of a single-point attachment of the ballast to the acrylic hardhat, with a shock cord in parallel to minimize the shock loading on the acrylic.

This package was successfully deployed on our second attempt, after one anchor pre-trip. The implosion was recorded on the DAT system after an elapsed interval of 33 min, with an estimated depth of 4280 ± 50 m, based on later analysis of the acoustic echos and the known bottom depth. The return package was sighted and recovered within another hour. It was found that the acrylic hardhat and glass sphere were completely destroyed, with only two small shards of acrylic, approximately 1/2 cm in diameter, found still clamped behind two of the bolts. Only one of the titanium frame crossmembers remained, and this one had been detached on one side. A cursory examination of the broken welds suggested that they were broken in tension rather than compression.

All of the steel through-bolts that held the acrylic to the Ti frame were found to be bent, some as much as $\sim 10°$, by shear loading on each side of the titanium T stem. Later examination of the rims of the titanium frame holes that had contained the high-tensile steel bolts showed conclusively that the bending of these bolts was due to forces directed radially outward from the center of the frame, indicating the the dominant forces were explosive rather than implosive. The titanium frame had yielded typically ~ 1 mm in these holes, but the vertical titanium section had retained its integrity as a tensile member of the mooring.

Visual examination of the kevlar and electro-optical riser cable bundles showed no damage, beyond a small nick in one of the kevlar splices which was attributed to its proximity to the sharp surface of the broken crossmember weld. No shards of glass or acrylic were evident on any of these riser surfaces, and none were found subsequently within the kevlar yarns or cable bundles. High density polyethylene, and polyvinyl chloride thimbles used to terminate the kevlar also showed no evident damage under visual inspection.

3.3 Third test

A third implosion test was conducted without any hardhat to determine a baseline acoustic profile for normalizing the profile obtained with the hardhat and frame. This was conducted successfully, with an elapsed descent time of 29 min. The implosion depth was later estimated to be 4470 ± 50 m, by bottom echos. Thus the final implosion was the deepest of the three, with almost 10% higher potential energy available than the shallowest implosion.

4 Results

4.1 Implosion Depth Relation

Orr and Schoenberg (1976) found an empirical relation between the FTR of a ground sphere and the implosion depth. Based on laboratory experiments with a pressure vessel, the dependence of the implosion depth on the FTR was found to be nearly linear. However, the fit of this laboratory curve to the actual field data of Orr and Schoenberg was imperfect, suggesting that the curve might be different under deep sea conditions as compared to a pressure vessel. Because of this possibility, the spheres for our test were ground to FTRs extrapolated from only the field data of Orr and Schoenberg. The FTR required to fit the laboratory curve for implosion depths of 4 km could actually lead to real implosions as deep as 4.8 km, beyond our site depth, if the deep-ocean behavior is different from that in the laboratory.

Figure 3 shows our results and those of Orr and Schoenberg (1976), along with two curves: the dashed line indicating the best fit for the laboratory data of Orr and Schoenberg, and the solid line a fit to only the deep ocean data. Our additional data clearly indicate that the laboratory tests do not adequately describe the dependence for the deep ocean implosions. However, the data do fit well to a straight line and it appears that glass spheres may be prepared for implosion to a precision of order 50-100 m depth for such tests.

The empirical dependence of the implosion depth on FTR for 43 cm housings similar to the Benthos Inc. type is found to be:

$$D \text{ (meters)} = 7.46 \times 10^4 \text{ (FTR} - 0.0230) + 2600 \qquad (1)$$

valid over the range 2 to 5 km and an FTR range of 0.0230 to 0.0265. The difference between this result and that measured in the lab may be attributable to many factors; one obvious one is the temperature difference, which could increase the relative strength of the glass in the ocean.

4.2 Acoustic Profiles

The acoustic profiles are shown in Figure 4, with the solid line indicating the profile of the deeper implosion, which had no hardhat or frame; and the dashed line that of the shallower implosion,

which had both. As mentioned above, the acoustic profile of the first test was not recorded, but both the second and third tests were successfully measured. The high-gain channel in both cases was saturated by the peak of the shock wave; thus Fig. 4 shows only the profiles recorded in the low-gain channel. The shallow depth of the hydrophone gave a prompt surface reflection which confuses the profiles $\sim$ 4 ms after the implosion onset; these reflections are not included in Figure 4.

The calibration of the pressure scale is shown in Pascals referenced to 1 m radius from the source, assuming spherical spreading. The absolute scale was determined from the results of Orr and Schoenberg (1976), using a fit to the magnitude of the underpressure pulses for the six 43 cm spheres they tested. The leading underpressure pulse is unaffected by acoustic attenuation since it is low frequency; it was found that the magnitude of this pulse was well-fit by a linear relationship with depth, allowing us to extrapolate to the implosion depths of our data.

Unfortunately, the hydrophone used to record the acoustic profiles was later found to have a ringing problem over the frequency range 6-10 kHz, and reduced sensitivity over the range 6-12 kHz. We have not yet attempted to measure the complex transfer function of the hydrophone, which might allow us to fully correct for these effects. However, such transfer functions can also have amplitude dependence which makes it difficult to calibrate highly impulsive events. For the present it is best to use the data in the range of 6-12 kHz with caution; however, the hydrophone manufacturer claims that the sensitivity is uniform over other portions of the spectrum up to $\sim$ 25 kHz.

The acoustic energy may be estimated by (Urick 1967):

$$E = \frac{4\pi}{\rho c} \int_0^T P^2(t)\, dt \tag{2}$$

where $P(t)$ is the measured pressure (referenced to $r = 1$ m here), ρc the density-velocity product for seawater, the 4π factor accounts for solid angle, and T is the duration of the acoustic event. Figure 5 shows the acoustic energy fluence as a function of time, and Figure 6 the cumulative total acoustic energy, both estimated from the surface measurements, assuming spherical symmetry.

The acoustic power spectra of the two pulses are shown in Figure 7. A number of hydrophone artifacts are present as discrete resonances apparent both in the time series and power spectra at $\sim$ 7 and $\sim$ 9 kHz, and possibly at their first overtones as well. The spectrum has not been corrected for this hydrophone response function. However, we have corrected for the known water-column attenuation, which is approximately quadratic in frequency above $\sim$ 5 kHz in our data, and amounts to $\sim$ 10 dB at the Nyquist limit.

The broad infall pulse produces the bulk of the lower frequency power, with a peak of about 600 Hz, slightly higher that that seen by Orr and Schoenberg (1976). The slope of the decay in the spectrum in the region below 5 KHz matches fairly well the average slope seen in the spectra of Orr and Schoenberg (solid line), whose spectra cut off at this frequency. In spite of the artifacts, it is evident that there is significant power in the shock wave pulse up to the Nyquist limit of the sampling used. In fact, the flat distribution at higher frequencies shows the impulsive nature of the

shock wave, and indicates that it would be *unresolved at our sampling interval*, if the frequency-dependent water-column attenuation were not present. This flattening may be contrasted with results described by Urick (1967), where explosive charges at these depths show spectra that fall off as power-laws with frequency above 600 Hz. It appears that implosions on large spheres may have inherently more high-frequency spectral content than explosive events of similar energy.

From Figures 5 and 6 it is apparent that the energetics of the implosion are dominated by the shock wave, even though the data are uncorrected for water-column attenuation. The total acoustic energy for both of our events is of order 45% of the available potential energy of the implosions. This contrasts rather strongly with the results of Orr and Schoenberg (1976), who found an average of 21% conversion to acoustic energy. Since energy goes effectively with the square of the peak pressure (Urick 1967), the acoustic efficiency will be underestimated if the shock wave pulse is undersampled. We suggest that the discrepancy here could be due in part to such sampling effects, but may also be related to the fact that our implosions took place at depths 20-70% greater than those of Orr and Schoenberg (1976).

4.3 Mechanical forces

Other than extrapolations of the measured acoustic pressure variation during the implosion events at the surface, we have two distinct pieces of evidence concerning the mechanical forces encountered in the near field. The first is the yield of the steel bolts used to anchor the hardhats into the titanium frame (and the yield and breaking of the frame itself), and the second is the shattering of the syntactic float at a distance of $\sim$ 16 m from the implosion.

4.3.1 Material yields

Based on the yields of the various materials used, each hole in the titanium frame, and the associated bolts, experienced forces of order 10 KN during the impulse which caused the yield. However, there is considerable uncertainty in converting this to mechanical energy by using products of the force and the yield distance, since the effective bearing surface area on the parts can only be roughly estimated. In spite of this uncertainty, a number of estimates by different methods suggest values as high as 10^6 Joule for this impulse, 2/3 of the total potential energy available. This exceeds both the estimate from surface measurements and the expectations from Orr and Schoenberg's results, and supports the suggestion that significant power in the initial shock is injected into very high acoustic frequencies that are absorbed in the near field.

4.3.2 Shatter of syntactic float

Such high frequency content may explain the apparent shattering of our float, although the evidence is less compelling since the history of the float indicates that it had had many pressure cycles, and rough handling before our use of it. If we estimate the peak overpressure in the shock

wave, correcting the surface measurements for the known transmission loss within our sampling frequency range, the implied stress is

$$P_{max}(r) = \frac{1}{r}\, P_{max}(1\text{ m})\, 10^{D\alpha(f)/20} \tag{3}$$

where $P_{max}(1\text{m})$ is the peak pressure referenced to 1 m, D is the depth in km, and $\alpha(f)$ is the spectral attenuation coefficient in dB km^{-1} at frequency f in Hz. The $1/r$ rather than $1/r^2$ dependence is characteristic of a spherical pressure wave: since the energy depends on the square of pressure, and it is the energy fluence which obeys a $1/r^2$ propagation law, the pressure must fall off as $1/r$.

For the implosion which caused the loss of our float, the peak pressure can be expected to be at least a factor of three higher than the measured surface peak pressure (both referenced to 1 m) based on the $\sim$ 10 dB loss in intensity at the highest frequencies measured, and this is probably a lower limit. Thus, from equation 3 for a distance of 16 m, $P_{max} = 4.6 \times 10^6$ Pa (about 660 psi). However, at 16 m distance, even frequencies of 1 MHz are only attenuated about 3 dB in the near field water column.(cf. Apel, 1987). Thus if the indications of the power spectra in Fig. 7 are correct, this stress estimate is also only a lower limit. Since even pure cast epoxy has a tensile strength of only a few thousand psi, the indications are that the pressure stress exceeded the tensile strength of the float.

Examination of the fractured surfaces of the float showed granularity and bubbles in the epoxy on scales of order 1 mm, all of which was apparently part of the construction of the material (typical sizes of the glass microspheres embedded in the epoxy matrix are of the order of 0.020 mm or less). This scale corresponds to a typical acoustic wavelength at 1 MHz. Some of the fractures followed interfaces between the different molded sections of the float, indicating that the shock wave was refracted by the density inhomogeneities within the float. This effect, combined with the possibility of resonant scattering by inhomogeneities with wavelengths characteristic of the incoming shock front, suggest that syntactic foam may be particularly susceptible to such damage.

4.3.3 Predicted mechanical shock-loading of other components

The damage to the float discussed in the previous experiment raises the issue of shock-loading of electronics contained within other housings of the array due to implosions. Two types of housings are presently planned for the array: the optical modules, housed in 43 cm diameter glass instrument housings, with the interior photomultiplier and electronics coupled mechanically to the housing via a thickness of $\sim$ 1/2 cm of silicone gel, and the central string controller, which is expected to be a 20 cm diameter Al tube of approximately 2.5 m length, with electronics contained in an internal rack-mounting system, with a number of nylon bushings between the rigid rack and the tube wall.

To make an estimate of the acceleration experienced by components within these housings, we treat two limiting cases: first, the resonant acceleration of an entire housing by an acoustic

pressure wave with wavelength of order twice the dimension of the housing. The other extreme is the very high-frequency case where the wavelengths are short enough to be treated by geometric optics. The first case should obtain for the underpressure wave and the second for the highest frequency components of the shock wave.

Resonant acceleration: For the optical modules, the strongest resonant coupling will occur from components in the pressure wave with time scales of ~ 0.5 ms, which is the same wavelength as the underpressure infall wave (not surprisingly, since this is caused by a 43 cm sphere).

For an implosion with a maximum underpressure point of P_U (re 1 m) Pascals, the resonant acceleration of an OM of the same diameter and mass M at a distance r will be

$$a_{res}\,(P_U; r) = \frac{1}{r}\,\frac{\epsilon\, P_U\, A}{M} \tag{4}$$

where the factor $\epsilon \leq 1$ is a coupling efficiency factor, and the PMT module cross section here is ~ 0.15 m. For $\epsilon = 50\%$, the acceleration for the deeper of our two implosions is 1200 m s^{-2} (120 g) at a distance of 10 m and a module mass of 25 kg. This factor is already quite large, probably enough to damage crystal oscillators permanently. If the coupling efficiency is near unity, accelerations $\geq$ 50g would be experienced out to ranges of $\sim$ 50 m. This could cripple a substantial part of the array if no vibration isolation is used for sensitive components.

Given the survival of the transponder in the first implosion test at a distance of 6 m from the implosion, there is evidence that electronics can survive in proximity to such an event. The transponder was somewhat shielded by the adjacent float spheres, and also the mechanical coupling to these spheres would provide a damping mass to its acceleration, but in any case an acceleration of a few hundred g is probable. We are in the process of acquiring documentation on the transponder electronics to evaluate this further.

The string mooring tension may help to damp the acceleration somewhat; however, the amplitudes of this oscillation are only a few mm even for high coupling efficiencies at 10 m, so the damping will probably not be large, and may even induce loads in the string riser elements which couple to other modules.

For the string controller, the estimates for bulk resonant coupling are more uncertain, but we can use the power spectrum in Fig. 7 to scale the peak of the 600 Hz pressure wave to the resonant frequency of an object of ~ 2.5 m length (about 300 Hz). The change from 600 to 300 Hz corresponds to a change of acoustic power of about -8 dB, or a loss of about a factor of 2.5 in peak pressure. The expected mass of the string controller is $\sim$ 250 kg, and the area $\sim 0.3\text{m}^2$ for a pressure wave traveling along the string. Thus the acceleration from an implosion at 10 m distance with a coupling efficiency of 50% would be $\sim$ 160 m s^{-2}, (16 g) which is probably survivable for most components.

Shock acceleration: The coupling of acoustic energy with wavelengths much smaller than the scales of the instrument housings proceeds by geometric optics. For normal incidence, the

transmission coefficient per interface (from medium i into medium j) is (cf. Rayleigh 1945):

$$T_{i,j} = 1 - \left[\frac{\rho_j/\rho_i - c_i/c_j}{\rho_j/\rho_i + c_i/c_j}\right]^2 \tag{5}$$

where ρ_i, c_i are the density and sound velocity in medium i. For coupling to instrument housings, at least two interfaces are encountered for coupling to internal electronics, so the total transmission will be (to first order) the product of the individual transmissivities. The coupling of pressure will depend on the square root of the transmission coefficient, again because of the relationship between energy and pressure. Thus equation (4) may be rewritten for the approximate acceleration due to acoustic coupling of the shock wave:

$$a_{shock}\,(P_{max}; r) \simeq \frac{1}{r}\sqrt{\prod_{i<j} T_{i,j}}\;\frac{P_{max}A_{eff}}{M} \tag{6}$$

where A_{eff} is the effective cross section of the module accounting for the integrals over non-normal angles of incidence, and the product is taken over all the interface transmission coefficients.

For the DUMAND optical module, the seawater-acrylic-seawater transition has a transmission coefficient of $\sim 95\%$ because acrylic is close in both density and velocity of sound to water. The seawater-to-glass transition has a transmission coefficient of ~ 0.4. Unfortunately it is difficult to estimate the velocity of sound in the silicone gel that couples the PMT to the sphere. However, assuming a speed of sound of 500 m s^{-1} for this gel, the transmission coefficient is ~ 0.15. If we use an effective area of 0.1 m^2 for the module, the implied acceleration at 10 m, for a peak overpressure of 10^8 Pa, is 10^4 m s^2 (1000 g), ignoring attenuation of the pressure wave in the gel. Thus it appears that at 10 m distance, we need an attenuation of 15-20 dB in this gel to decrease the shock loading to tolerable levels.

5 Discussion: Implosion Dynamics

The evidence from the data strongly suggests that the implosion event forms a fully developed jump-shock, which has the property that pressure is effectively discontinuous across its surface, leading to the observed impulsive acoustic event with strong high-frequency components. The requirement for developing such a shock is that the initial impact of the infalling material be at velocities in excess of the velocity of sound in the medium. This then provides the momentum pileup in the shock front which drives up the local pressure within the front so that the acoustic velocity in this region is significantly higher than in the pre-shock fluid. Such conditions thus lead to the inherent steepening of the leading pressure gradient as the acoustic Fourier components of the shock are trapped in the high pressure region. In this section we digress briefly to consider analytically whether these conditions appear to be fulfilled in these implosions.

5.1 Qualitative description

Before developing analytic results for the implosion parameters, it is useful to describe the sequence qualitatively. To do this, first consider an ideal case where there is no glass shell present, but a pressure-free cavity of 43 cm diameter is allowed to collapse. As the collapse begins, the initial pressure drop begins to propagate radially out as an acoustic wave. Within this radius, the entire water mass is beginning to accelerate radially inward, and the continuity equation indicates that, as the infalling surface of the cavity decreases in area as $1/r^2$ relative to its initial surface, the velocity must increase at the same rate. Thus both the pressure gradient, and the radial gradient in the area contribute to the acceleration of the infalling water.

As the water mass meets at the center, an acoustic compression wave is formed from the momentum of the collision, and this begins to propagate radially out. However, its velocity is retarded because it is moving upstream through the still infalling material above it. Thus, relative to the onset of the underpressure pulse, one expects it to be delayed by the infall time, plus the acoustic velocity out of a sphere radius, plus an additional delay due to the infall retardation. The relaxation time of the infalling material will be of order the acoustic transit time of the sphere, a few hundred microseconds, and after this time the outgoing compression wave will continue at the acoustic velocity. However, during transit of the infall region, the delay can be substantial if the mean velocity is comparable to the acoustic velocity. If the infall is supersonic, such effects will lead to a substantial delay of the outgoing shock wave because the modes are effectively trapped within the supersonic relaxation region until the infall motion is complete.

5.2 Semi-analytic Description

Here we analyze the infall of the water into a pressure-free spherical cavity, initially ignoring the glass shell and assuming spherical symmetry, and incompressibility for the water. The approach is denoted a semi-analytic one since we will depend somewhat on the characteristics of the measured profile of the infall pressure. The treatment is not intended to be accurate for velocities that approach the acoustic velocity of water.

5.2.1 Infall Velocity

We approximate the observed initial pressure drop (the first 0.5 ms in Figure 4) of the deeper of our two implosions by a linear gradient in time:

$$P(t) = -Kt \tag{7}$$

where the constant K can be evaluated from figure 4 to be $K \simeq 8 \times 10^9$ Pa s^{-1} re 1 m. Actually, it will be more convenient to reference the dynamical variables to the initial cavity radius $R_0 = 0.21$ m, so we use equation 3 to get $K_0 = K/R_0 = 3.8 \times 10^{10}$ Pa s^{-1}.

From Bernoulli's Law we can relate the fluid velocity at R_0 to this measured pressure drop:

$$P(t) = -\frac{\rho u^2(t)}{2} \tag{8}$$

where the pressure has been referenced to ambient pressure. Combining equation 7 and equation 8, we find the velocity as measured at R_0:

$$u_0(t) = \sqrt{\frac{2K_0}{\rho}}\, t^{1/2}. \tag{9}$$

Just outside the infalling surface (again ignoring the glass shell) the continuity equation (constancy of the product of area and velocity) then implies that

$$u_r(t) = \frac{dr}{dt} = u_0(t)\frac{R_0^2}{r^2} \tag{10}$$

where the variable r now refers to the radius of the infalling surface. This provides a separable equation which may be integrated in t and r:

$$\int_{R_0}^{r} r^2\, dr = \sqrt{\frac{2K_0}{\rho}} \int_0^t t^{1/2}\, dt \tag{11}$$

The result is:

$$r(t) = \left[R_0^3 - 2R_0^2\sqrt{\frac{2K_0}{\rho}}\, t^{3/2}\right]^{1/3} \tag{12}$$

and this may be inverted to get the time T_c that the infall reaches the sphere center:

$$T_c = \left(\frac{R_0}{2}\sqrt{\frac{\rho}{2K_0}}\right)^{2/3}. \tag{13}$$

Using the parameters for our second implosion, the infall time is estimated from this equation to be ~ 540 μs, which is very close to what is observed in Fig. 4. At this point the acceleration stops, and the expansion of the compressed region causes the change in sign of the first derivative of the pressure as observed in Fig. 4. However, as discussed above, the shock wave will not appear until after an additional lag due to relaxation effects, and the transit time out of the sphere. The actual leading edge of the shock wave appears at about 1200 μs, implying that the dynamical effects during the production of the shock wave after the initial infall are significant, since the transit time out of the sphere radius is only about 120 μs.

The infall radius and velocity as functions of time are shown in Figure 8 (a) and (b) for the deeper of the two implosions of Fig. 4. The radius at which the velocity becomes supersonic may be determined by setting the left hand side of equation (10) equal to c and solving for the radius at the time the infall reaches the center. For the example above, the supersonic infall radius extends out to 7 cm, as is shown by Figure 8(c) which plots the infall velocity against infall radius.

5.3 Caveats

Obviously this analysis is subject to a number of limitations, which we mention here. First, we have ignored effects of the compressibility of water; however, such effects will be of critical importance in the development of the shock wave. Compressibility plays a role in the regions of subsonic velocity as well, leading to some rebound effects in the initial underpressure wave. However, for our purposes, which are primarily to demonstrate that conditions for shock formation are present, water may be considered incompressible to first order.

Two other effects which are ignored in this initial treatment are the glass shell, and the internal pressure of the sphere. We discuss both in some detail in the remainder of this section.

5.3.1 Effects of glass shell

The velocity of shear waves in pyrex glass at atmospheric pressure is ~ 3300 m s^{-1} and therefore a time scale of ~ 0.2 ms is required for fractures to propagate from one side of the sphere to the other. Thus the glass initially provides some resistance to the infall while the fracturing process continues. This effect may be the cause of the initially lower gradient in the pressure function seen in Fig. 4. There is a distinct change in slope at a time of ~ 160 μs after the infall onset, of the right order of magnitude for the initial stages of the glass fracturing event.

Once the fracturing has crossed the sphere, no pressure support can be maintained, and the implosion should proceed in a manner similar to that described above, with the glass being driven out in front of the infalling water surface. However, the higher density of the glass as compared to water will also slow down the infall somewhat, since the velocity depends on $\rho^{-1/2}$. We have made estimates of the density of glass agglomerations recovered from the remains of hardhats that survived sphere implosions similar to ours, and these fall in the range $1.2 - 1.7$ gm cm^{-3}. Thus the glass might be expected to impede the infall rate by $\sim 30 - 40\%$, if all of the infall volume were an admixture of glass and water. However, the glass only comprises 1/5 of the sphere volume, and thus the square root of the average density only increases by $\sim 10\%$.

Another likely result of the fracturing event is to introduce asymmetry in the infall geometry, but it was found by Orr and Schoenberg (1976) that the spheres imploded in pressure vessels yielded glass which was completely fractured to sand-sized particles. Glass recovered from deep-ocean implosions shows a particle size spectrum ranging from sand down to micron sizes. The absence of large pieces of glass suggests that enough symmetry is maintained during the implosion so that nearly complete fracturing can still take place.

However, the volume of the glass involved is sufficient to produce a sphere of radius ~ 13 cm at the center of the implosion if it retained its pre-fracture density, which is not the case. Using the average of the densities that we have reported above, the volume of the fractured glass corresponds to a sphere of order 15 cm radius, 3/4 that of the entire pre-implosion radius. Thus the presence of the glass is clearly important to the dynamics of the shock wave formation, and further complicates interpretation of the pressure signature, since it occupies the volume in which

the shock wave is generated.

We note in passing that the potential energy of the event is a small fraction of what would be required to fuse this volume of glass, even if the conversion to thermal energy were 100% efficient.

5.3.2 Effects of internal pressure

The gas internal to the sphere was neglected above in calculating the infall velocities. Here we assess its effects on the implosion dynamics.

The critical radius r_C at which internal pressure effects can be expected to become important is of order

$$r_C = R_0 \left(\frac{P_I}{P_A} \right)^{1/4} \tag{14}$$

where we have assumed the ideal gas law with adiabatic index $\gamma = 4/3$, the initial internal pressure is P_I, and P_A is the ambient pressure ($P_A \simeq D \times 10^7$ Pa at D km depth).

As an example, if the sphere had an initial internal pressure $P_I = 1$ atm, the compressed internal gas would reach 20% of the ambient pressure for 4.5 km depth at a radius of ~ 7 cm, and would equal the ambient pressure at ~ 4.5 cm. Thus an internal pressure of 1 atm might lead to some moderation of the infall velocity near the supersonic radius, possibly decreasing it somewhat. Initial internal pressures in our tests were 0.22 atm and we conclude that they had probably had little effect on the dynamics of the shock formation, as compared to effects due to the matrix of fractured glass the occupies the central volume as the shock wave begins to form. It is worth noting that Orr and Schoenberg used two different internal pressures in the spheres they studied, 0.7 atm and 0.07 atm, and they could see no difference in the behavior of the acoustic signature of the two different types, a result that supports our conclusion above.

6 Conclusions and recommendations

A rigid titanium frame was successfully used to protect tensile and electro-optical cables in a riser bundle similar to that planned for use in the DUMAND array, from damage due to the energetic implosion of a 43 cm Benthos Corp. glass instrument housing. The frame itself was damaged in its weakest member, and the explosive forces present were strong enough to cause yield of portions of the frame, but the protective function of the frame was still intact, and its strength as part of the tensile riser of the mooring used was also retained. It is recommended that the crossmember of the frame be strengthened since it is preferable to have the frame remain intact to avoid having the sharp surfaces of the broken frame near the kevlar riser following an implosion event.

We have indirect evidence that similar glass housings within a distance of ~ 6 m of an imploding sphere did not undergo sympathetic implosions, and direct evidence that a sphere within 24 m of an imploding sphere remained intact. Since some of the distances between spheres within the

DUMAND array could be less than 6 m, further tests should be done to determine the safe distance at which a second sphere can survive.

A syntactic float within 16 m of an implosion was apparently shattered by the event, possible due to much higher near-field pressure gradients than are measured at the surface. The surface acoustic profiles do show power up to the Nyquist frequency due to the shock-wave pulse, indicating that higher frequencies were also present. A simple qualitative analysis of the development of the shock wave also indicates that shock conditions, requiring supersonic collision of the infalling material, are strongly satisfied in such an implosion event. This analysis also supports the hypothesis that the near field pressure peak may be dominated by very high frequencies which are absorbed before reaching the surface. Thus it is recommended that the top float for each string be separated to a distance of $\gg$ 16 m above the last glass sphere. The use of glass floats in the array should be considered as well, but the problem of sympathetic implosions should then be investigated in more detail. Mechanical isolation of the most shock-sensitive components in the OMs appears to be necessary if they are to survive the implosion shock within a distance of a few tens of meters or more.

Because of the probable presence of very high frequencies in the near field around an implosion event, it may be worthwhile to develop high frequency attenuation masks around the hydrophones in the array, for frequencies above the Nyquist sampling limit of the recording system. The maximum overpressure that is possible in the near field event could correspond to an increase in depth of up to 8 km momentarily; thus the peak pressure may exceed the rating of the hydrophones, and an attenuator may help reduce this.

We wish to thank Sam Raymond of Benthos Corporation for his invaluable assistance in preparing the implosion spheres for this experiment. We also thank Capt. Jack Ross, skipper of the vessel *Capt. Jack*, of Keauhou Bay, Hawaii Island, for his help in staging the deployment operations, his amazing stamina, and continual good cheer.

References

Apel, J. R., 1987. Principles of Ocean Physics. (London: Academic Press).

O'Connor, D. J., 1990. Unpublished Dissertation, University of Hawaii.

Orr, M., and Schoenberg, M., 1976. Journ. Acous. Soc. Am. 59, 1155-1159.

Raymond, S. O., 1975. IEEE Ocean '75, 537-544.

Lord Rayleigh, 1945. The Theory of Sound, vol II, (New York: Dover).

Urick, R. J., 1967. Principles of Underwater Sound for Engineers. (New York: McGraw-Hill).

Figure Captions

Figure 1: Implosion sphere geometry. The indicated dimension is the wall thickness at the flat; the ratio of this to the sphere radius determines the flat-thickness ratio (FTR).

Figure 2: (A) A schematic of the setup for the first implosion test. The wavy lines indicate schematically the mock electro-optical riser elements, which were not under tension in the test. (B) Schematic for the second test.

Figure 3: Implosion depth vs. the Flat Thickness Ratio (FTR) for nine 43 cm sphere deep-ocean implosions. The solid line is a fit to the deep ocean data; the dashed line a fit to Benthos pressure-vessel data for comparison.

Figure 4: Time profiles of the two implosions for which they were recorded. The apparent oscillation after the positive peak is due to a hydrophone artifact. The pressure has been referenced to ambient pressure at a distance of 1 m from implosion center.

Figure 5: Total acoustic energy fluence of the two events, assuming spherical symmetry. The sample duration was about 20 microseconds.

Figure 6: Cumulative total acoustic energy for the events, also assuming spherical symmetry.

Figure 7: Acoustic power spectrum for the two events, referenced to an arbitrary baseline power. The data has been corrected for seawater attenuation over a distance of 4.2 km. The solid line indicates the average slope for Orr and Schoenberg's 1976 data for frequencies below 5 KHz. The dashed extrapolation of this line shows that the higher frequency data does not continue this trend. The apparent resonance peaks in the spectrum at 7 and 9 KHz, and the structure above 10 KHz are due to hydrophone artifacts, and the slope above 20 KHz is uncorrected for the falling hydrophone sensitivity.

Figure 8: Predicted time dependence of (a) the infall radius, and (b) the infall velocity, for the deeper of our two implosions. (c) Infall velocity as a function of infall radius for same implosion. See text for details of predictive model.

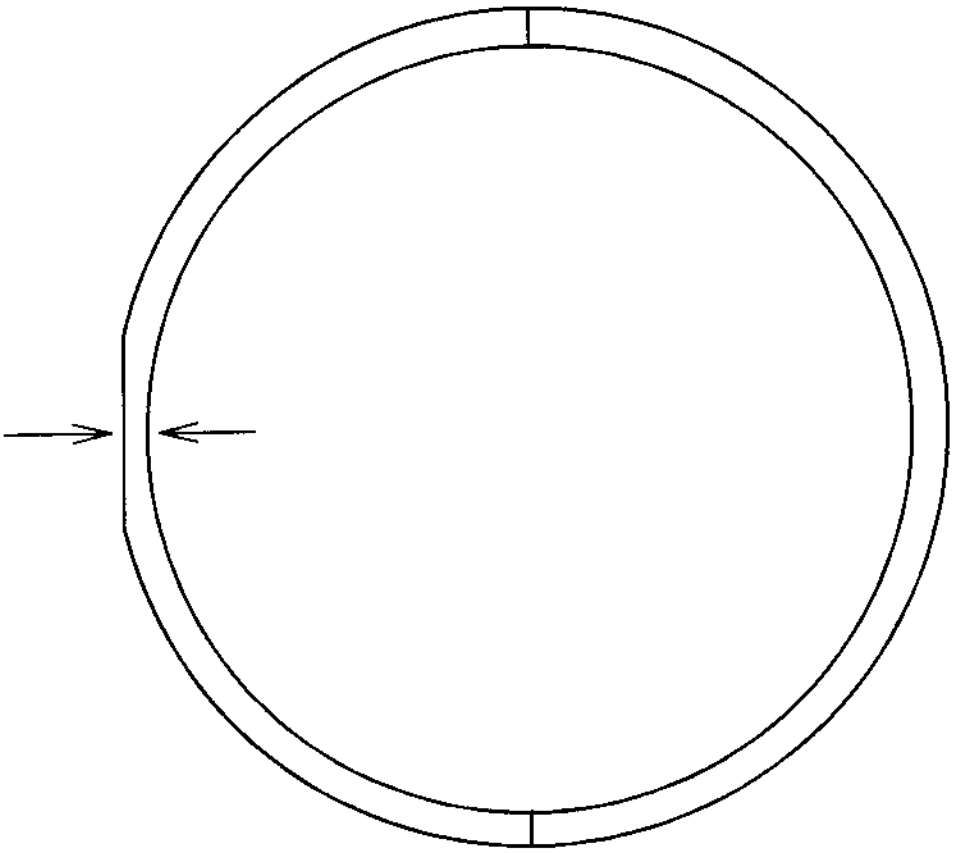

FIG. 1

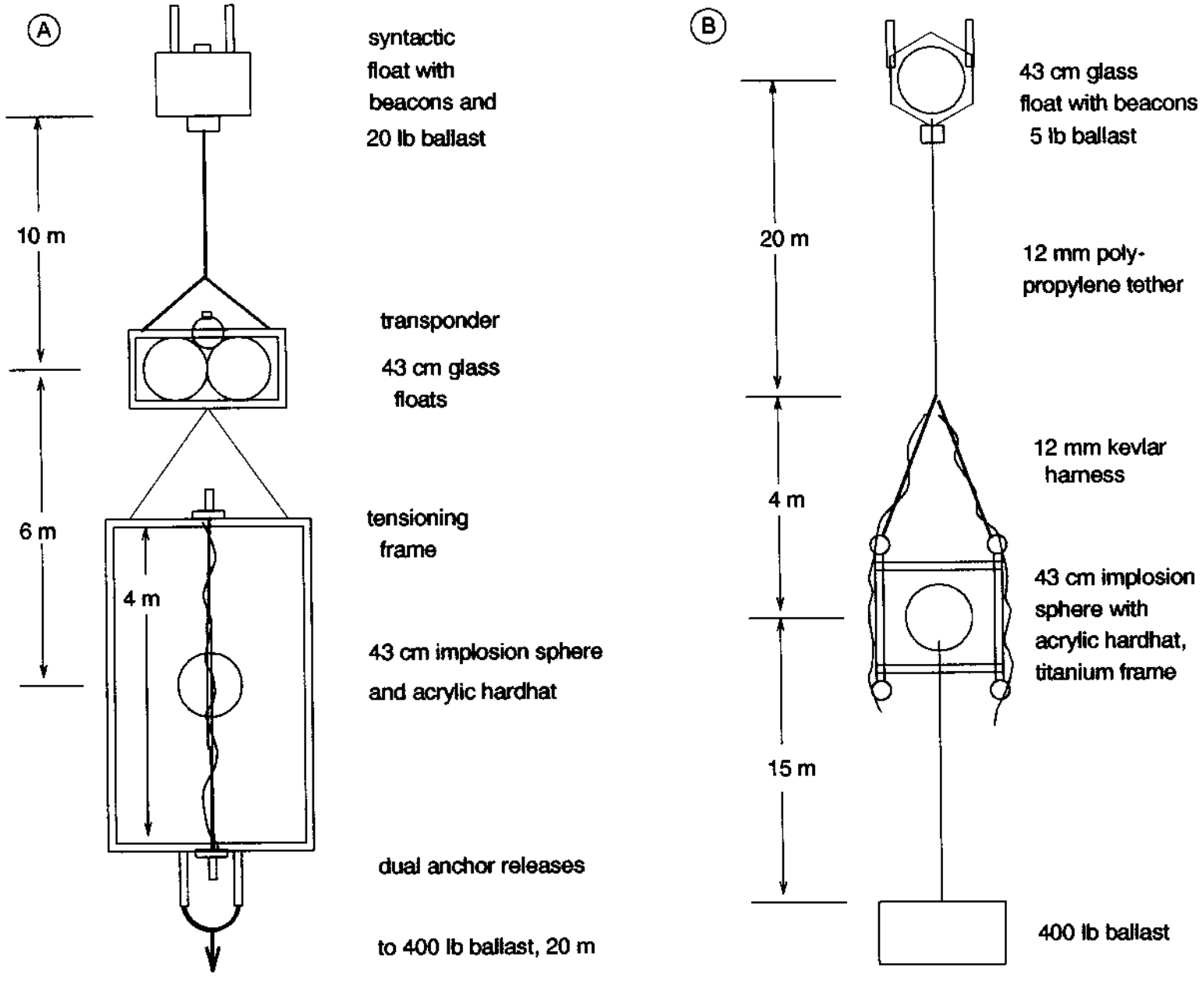
A
10 m
6 m
4 m
syntactic
float with
beacons and
20 lb ballast
transponder
43 cm glass
floats
tensioning
frame
43 cm implosion sphere
and acrylic hardhat
dual anchor releases
to 400 lb ballast, 20 m
B
20 m
4 m
15 m
43 cm glass
float with beacons
5 lb ballast
12 mm poly-
propylene tether
12 mm kevlar
harness
43 cm implosion
sphere with
acrylic hardhat,
titanium frame
400 lb ballast

FIG. 2

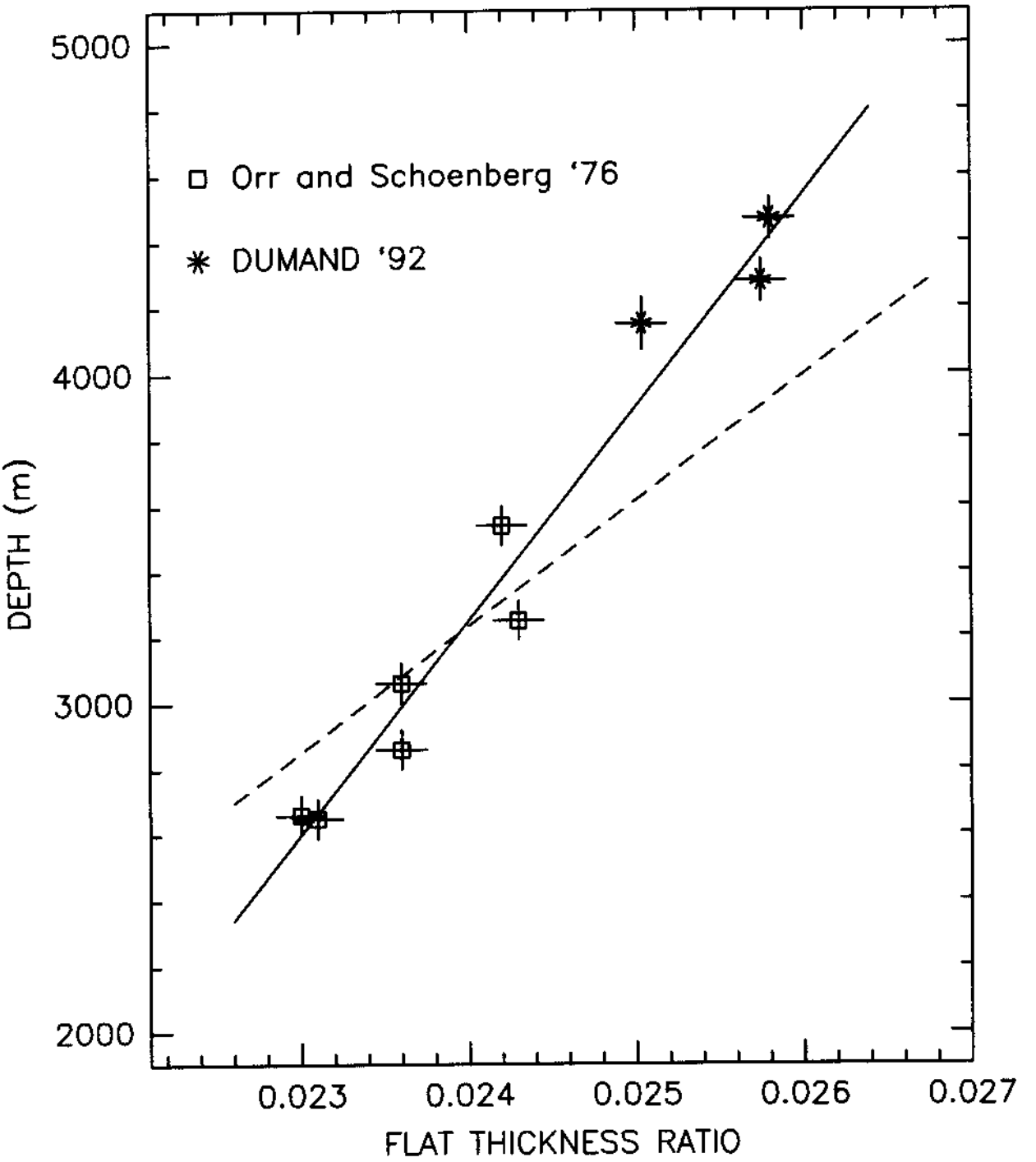
5000
4000
3000
2000
DEPTH (m)
Orr and Schoenberg '76
DUMAND '92
0.023
0.024
0.025
0.026
0.027
FLAT THICKNESS RATIO

FIG. 3

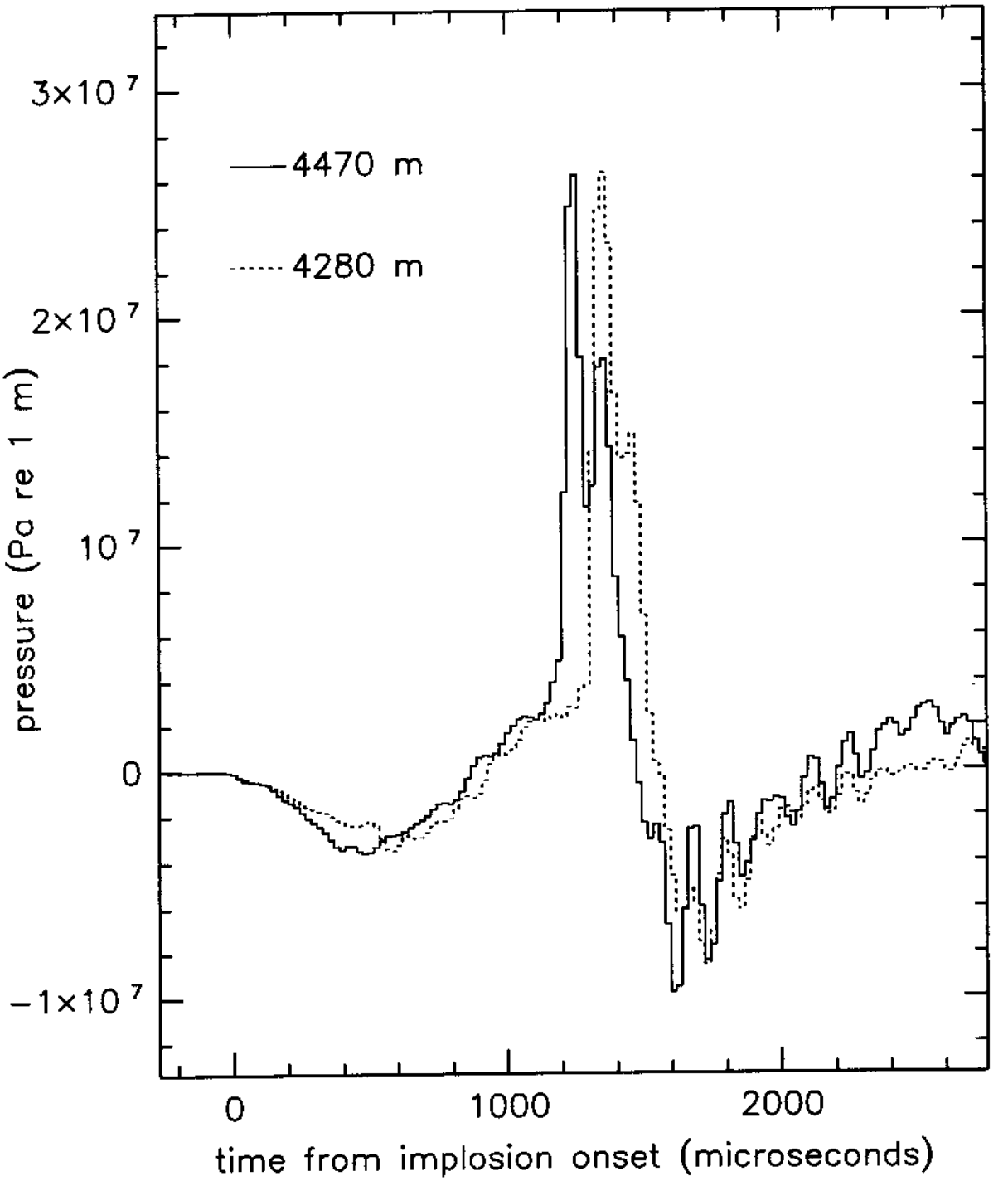
3×10 7
2×10 7
10 7
0
−1×10 7
4470 m
4280 m
pressure (Pa re 1 m)
0
1000
2000
time from implosion onset (microseconds)

FIG. 4

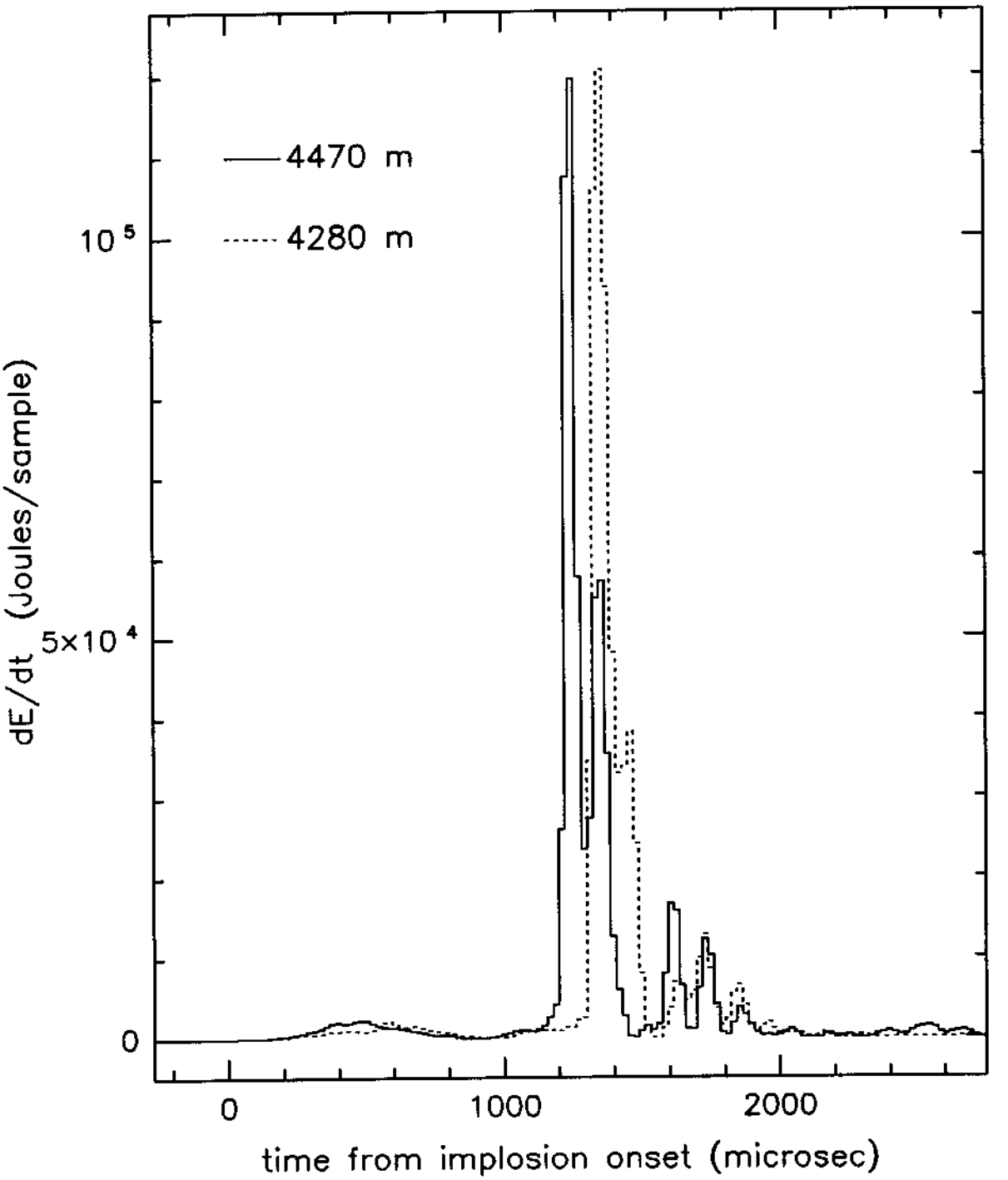
4470 m
4280 m
10 5
5x10 4
0
dE/dt (Joules/sample)
0
1000
2000
time from implosion onset (microsec)

FIG. 5

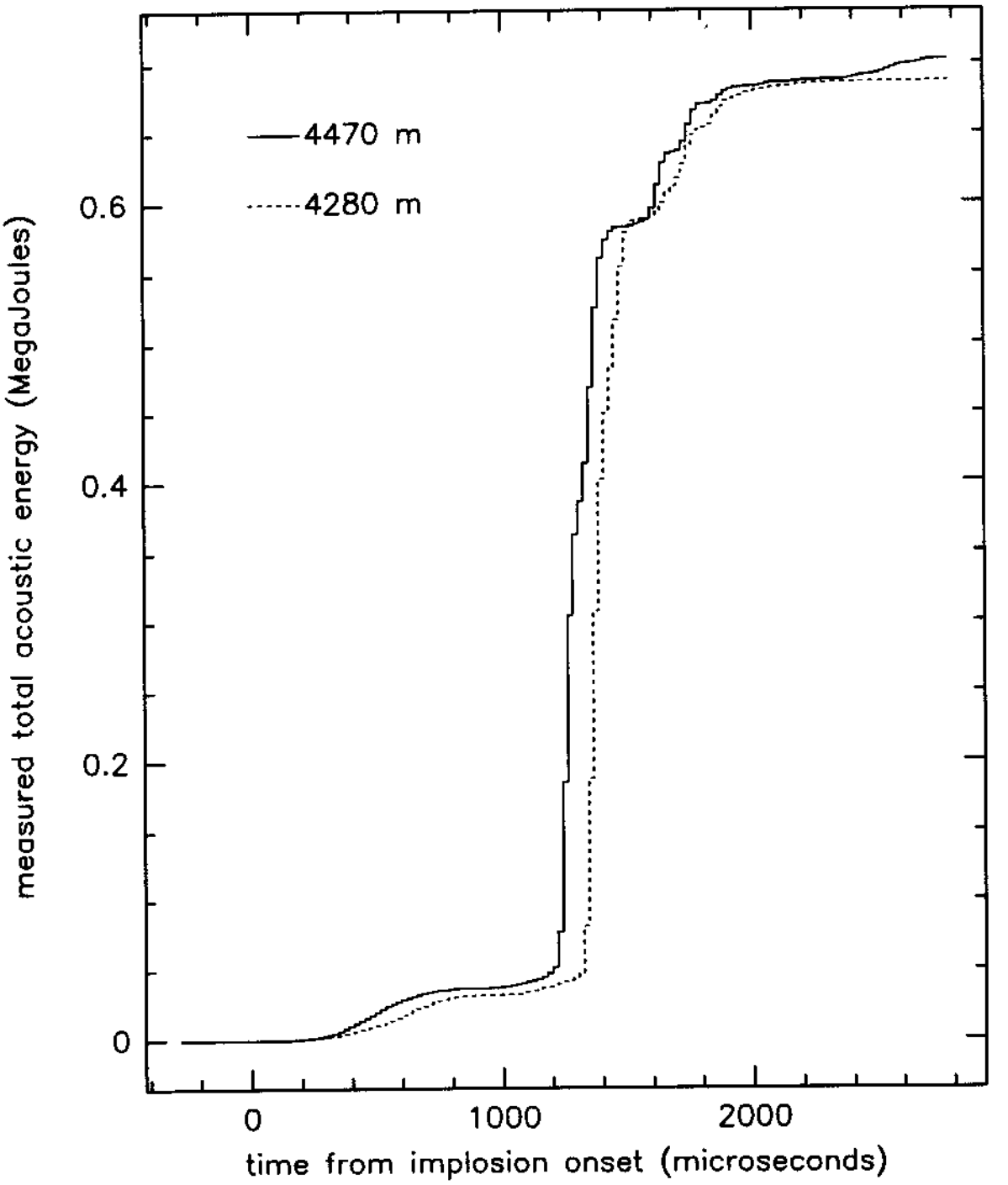
4470 m
4280 m
0.6
0.4
0.2
0
0
1000
2000
measured total acoustic energy (MegaJoules)
time from implosion onset (microseconds)

FIG. 6

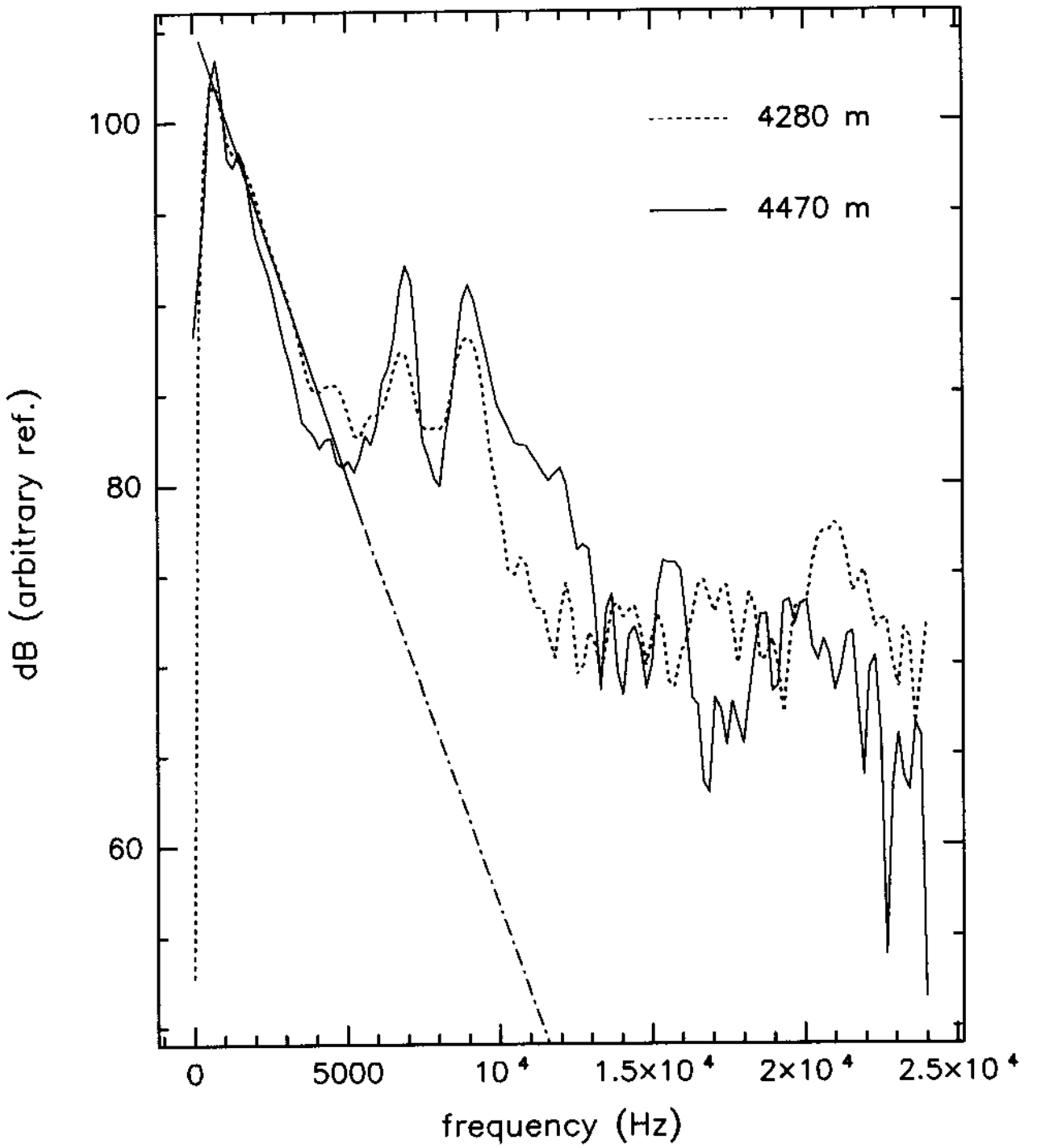
4280 m
4470 m
100
80
60
dB (arbitrary ref.)
0
5000
10 4
1.5×10 4
2×10 4
2.5×10 4
frequency (Hz)

FIG. 7

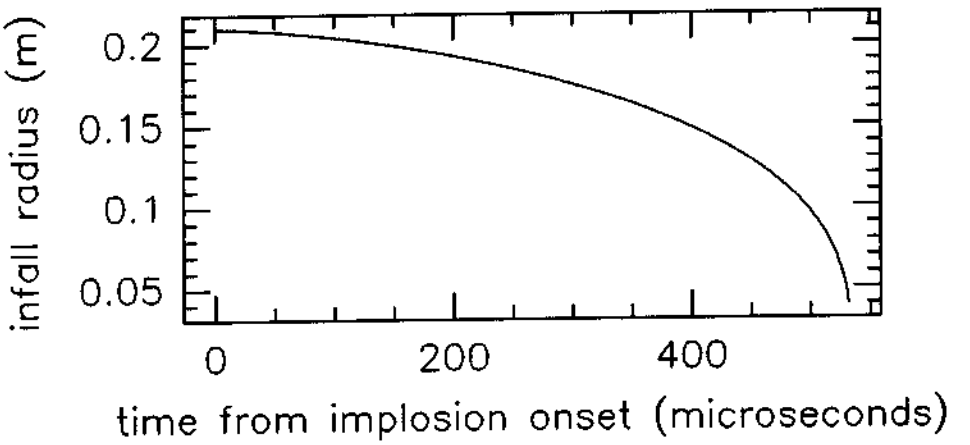
infall radius (m)
0.2
0.15
0.1
0.05
0
200
400
time from implosion onset (microseconds)

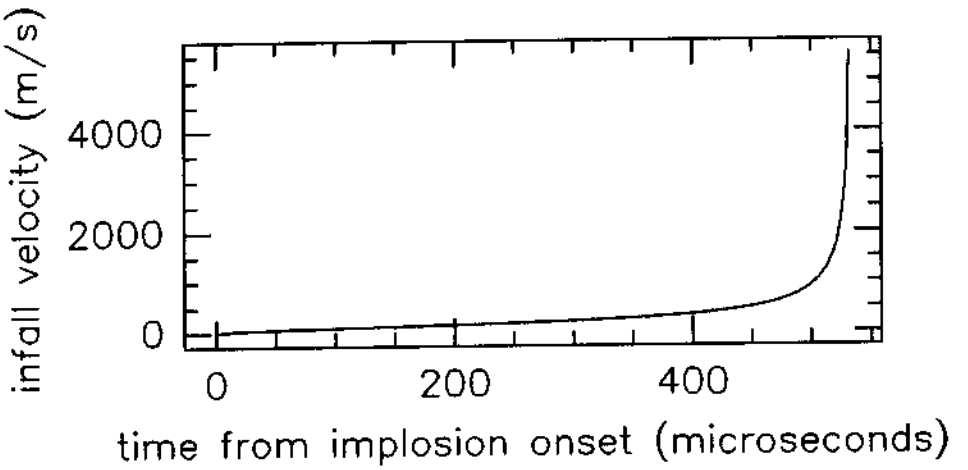
infall velocity (m/s)
4000
2000
0
0
200
400
time from implosion onset (microseconds)

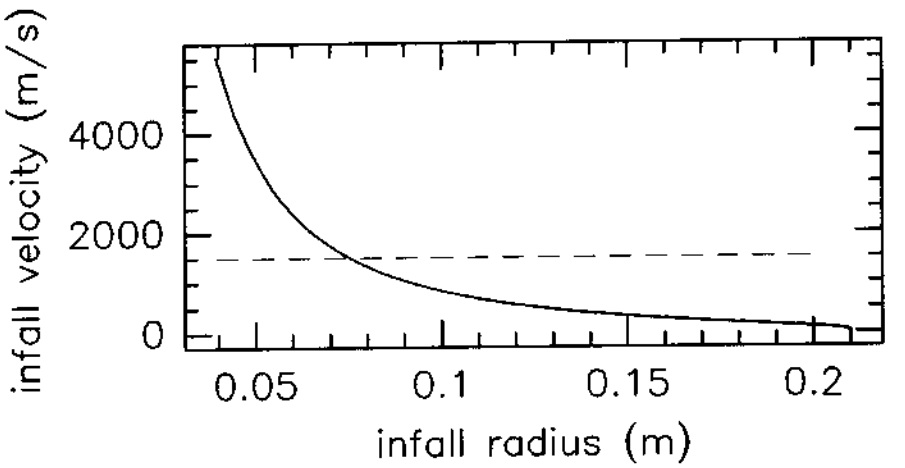
infall velocity (m/s)
4000
2000
0
0.05
0.1
0.15
0.2
infall radius (m)

FIG. 8